Real-time path integrals for quantum dots: Quantum dissipative dynamics with superohmic environment coupling

A. Vagov,[1] M. D. Croitoru,[1] M. Glässl,[1] V. M. Axt,[1] and T. Kuhn[2]
[1]*Institut für Theoretische Physik III, Universität Bayreuth, D-95440 Bayreuth, Germany*
[2]*Institut für Festkörpertheorie, Westfälische Wilhelms-Universität Münster, D-48149 Münster, Germany*
(Received 15 November 2010; published 16 March 2011)

Based on a representation of the functional integral as the time evolution of the augmented density matrix we have worked out an implementation of the real-time path integral approach that is applicable to the dynamics of quantum dissipative systems with superohmic coupling to the environment. As a prototype for such a system we consider a laser-driven strongly confined semiconductor quantum dot coupled to acoustic phonons. First applications of this approach to quantum dot systems have already been published. Here, we provide a detailed description of the implementation, including a discussion of numerical issues and extend the formalism from two-level quantum dot models with a pure-dephasing type carrier-phonon coupling to the case of multiple electronic levels. The method allows for numerically exact calculations of the dot dynamics at strong dot-phonon and dot-laser coupling and at long times, usually inaccessible by other approaches.

DOI: 10.1103/PhysRevB.83.094303 PACS number(s): 03.65.Yz, 78.67.Hc, 42.50.Md, 78.20.Bh

I. INTRODUCTION

The functional integration method is a well-known tool in the theory of dissipative systems.[1,2] It is particularly easy to formulate for models where carriers are linearly coupled to harmonic-oscillator degrees of freedom such as environment phonons. In principle the method is capable of providing numerically accurate results in regimes inaccessible to other approaches. However, numerical real-time path integrations typically have to face a number of difficulties. The most severe of them is the so-called dynamical sign problem which refers to the difficulty to sum up accurately a huge number of paths of similar weight that almost cancel out due to the summation over different phase factors. An elegant and numerically reliable way to overcome this problem has been developed in Refs. 3–7 for a certain class of dissipative systems for which initial value problems have been discussed without external driving. As practical calculations with this scheme mainly aimed at applications in the field of chemical physics, the focus of these studies has been exclusively on systems with ohmic or subohmic coupling types, for which physical problems, such as dynamic localization and the crossover between coherent and incoherent dynamics, have been studied. Here, as usual, a system environment coupling is called *subohmic* when the spectral density of the effective coupling strength $J(\omega)$ scales in the low-frequency limit as $J(\omega) \propto \omega^a$ with $0 \leqslant a < 1$. For $a = 1$ it is called *ohmic* while the case $a > 1$ is referred to as *superohmic*. As will be shown below the application of numerical path integrals in the superohmic case requires a special treatment due to peculiarities of this type of coupling.

The pure dephasing type carrier-phonon coupling in strongly confined semiconductor quantum dots (QDs) represents a prominent example for a system with superohmic coupling.[8–14] The rapid development of experimental methods for studies of the ultrafast dynamics in such nanosized samples[15–20] continues to stimulate interest in the detailed theoretical simulation of the time evolution of these systems. Most of those experiments study the evolution in strongly nonlinear regimes, when a system is driven by external light of high intensities and many prospective applications of QD systems, in turn, rely on nonlinear properties as, e.g., Rabi oscillations. In addition the dynamics is strongly influenced by the interaction between the optically active carriers and other excitations in the media. For many QD systems the coupling between QD carriers and phonons in the embedding media provides the main dephasing mechanism in the ultrafast time regime. Furthermore, in many real situations the effective carrier-phonon coupling is not weak, especially at elevated temperatures.

The theoretical analysis of the dynamics when both the light-dot and the media-dot coupling are strong is a nontrivial task since one usually cannot identify a small parameter in the system. The genuine non-Markovian nature of the dynamics, reflected in many unusual features such as an experimentally observed nonmonotonic temperature dependence of the initial decay,[13] or a phonon-induced renormalization of the Rabi frequency,[21,22] provides an additional challenge as the influence of the environment cannot be captured by simple rates. Most theoretical approaches employed in the analysis of QD dynamics account fully for the dot-light coupling, but treat media-dot couplings within approximations which are explicitly or implicitly perturbative. For example, the correlation expansion method for the density matrix[21–23] or the two-time Green's function approach[24] contain arbitrary orders of the phonon coupling constant. However, not all terms in the perturbation expansion over the phonon coupling are taken into account, similarly to a summation of certain selected diagram classes. The noninteracting blip approximation (NIBA) and its improvements introduced in studies of quantum dissipative systems[1] implicitly employ similar approximations. The main assumption in the NIBA is that the phonon subsystem is not affected by the QD state, remaining in the thermal equilibrium during the evolution. This approach is believed to work rather well for ohmic and subohmic phonon couplings, but its validity for the superohmic case is questionable.[2] Indeed, it has been shown that the backaction of nonequilibrium phonons on the dynamics of QDs can be significant for

certain excitation conditions.[23,25] Approximate methods often yield qualitatively and, in some cases, quantitatively correct results. However, their validity is unclear in the limits of strong coupling, high temperatures, and long time dynamics. The real-time path integral implementation presented here can be used as a benchmark for standard approaches that make use of approximations as has been done for testing the range of validity of the density-matrix method in Ref. 26.

In this work we present an implementation of the numerical path integral method that is able to deal with superohmic couplings. We shall explicitly formulate the theory for semiconductor quantum dots with few carrier states coupled with external optical pulses and environment phonons which is certainly one of the major target systems for our approach. A dissipative system with superohmic coupling possesses a number of specific properties that are not found in systems with other coupling types. An important example is the existence of ever lasting polaronic complexes that strongly affect the spectral and dynamical properties of a QD. The polaron stability is related to asymptotic properties of the time dependence of the memory kernel that governs the interaction induced dynamics of carriers and phonons. As we shall demonstrate, these properties make the superohmic case particularly suitable for the analysis by path integral calculations, so that reliable results can be obtained at arbitrary long times.

The paper is organized as follows. In Sec. II we outline the model that is considered here. It constitutes a prototype for a system with superohmic coupling and describes a QD that is coupled to phonons and driven by external light pulses. Our numerical approach is presented in detail in Sec. III. Main formulas of the discretized version of the path integral for the special case of a two-level model are summarized in Sec. III A. A detailed derivation generalized for a multiple level system is given in the Appendix to make it easier for the reader to focus on the numerical algorithm. Section III B is devoted to the discussion of the memory truncation scheme and Sec. III C describes our numerical algorithm which utilizes this approximation in a controlled way. In Sec. IV we give a few illustrations of our method which are presented here mainly for benchmarking purposes and to show, how different physical excitation conditions and numerical issues of convergence and efficiency are interrelated. The major conclusions are formulated in Sec. V.

II. QUANTUM DOT MODEL

The dynamics of strongly confined semiconductor quantum dots are usually described within a model that accounts for few carrier states linearly coupled with phonons and light. When the electronic energy levels are well separated and the energy gaps are incommensurate with phonon frequencies, the phonon influence on the dynamics is dominated by the pure dephasing mechanism where phonon-assisted transitions between the carrier states are negligible. In many practical situations the model can be further restricted to account for only two optically active electronic levels that are resonantly coupled by external laser light pulses. When the frequency of the light source is close to the exciton energy gap one can use the rotating wave approximation (RWA) and, if in addition the light source is coherent and has a sufficiently high intensity, the light field can be modeled as a classical field. Under these conditions the relevant Hamiltonian is given by the laser-driven two-level independent Boson (TLIB) model:

$$\widehat{H} = \hbar\frac{\Omega}{2}(\widehat{\sigma}_z + \widehat{1}) + \frac{1}{2}(\widehat{\sigma}_z + \widehat{1})\hbar\sum_{\mathbf{q}}(\gamma_{\mathbf{q}} b_{\mathbf{q}}^{\dagger} + \gamma_{\mathbf{q}}^{*} b_{\mathbf{q}}) + \hbar\sum_{\mathbf{q}}\omega_{\mathbf{q}} b_{\mathbf{q}}^{\dagger} b_{\mathbf{q}} - \mathbf{d}\mathbf{E}(t)\widehat{\sigma}_{+} - \mathbf{d}^{*}\mathbf{E}^{*}(t)\widehat{\sigma}_{-}, \quad (1)$$

where Ω is the energy gap between the two electronic states. The ground state is taken as zero of the energy. $\mathbf{d}$ denotes the transition dipole for the transition between the two electronic states, while $\mathbf{E}$ is the laser field which is assumed in the form $-\mathbf{d}\mathbf{E}(t)/\hbar = f(t)e^{-i\omega t}/2$, with $f(t)$ being a real envelope function. $\widehat{\sigma}_{\pm} \equiv \widehat{\sigma}_x \pm i\widehat{\sigma}_y$, where $\widehat{\sigma}_x, \widehat{\sigma}_y, \widehat{\sigma}_z$ are Pauli matrices that act on the electronic subspace with the basis states $|0\rangle$ and $|1\rangle$. An extension to more than two levels is worked out in the Appendix. $\omega_{\mathbf{q}}$ is the frequency of a phonon that belongs to the phonon mode labeled by the mode index $\mathbf{q}$ and $b_{\mathbf{q}}$ ($b_{\mathbf{q}}^{\dagger}$) are the corresponding phonon annihilation (creation) operators. Finally, the exciton dot-phonon coupling $\gamma_{\mathbf{q}}$ is the difference between electron-phonon and hole-phonon constants, $\gamma_{\mathbf{q}} = \gamma_{\mathbf{q}}^{e} - \gamma_{\mathbf{q}}^{h}$.

An important quantity that can be derived from $\gamma_{\mathbf{q}}$ and the dispersion relation $\omega_{\mathbf{q}}$ is the spectral density

$$J(\omega) = \sum_{\mathbf{q}} |\gamma_{\mathbf{q}}|^2 \delta(\omega - \omega_{\mathbf{q}}). \quad (2)$$

Hamiltonians of the form Eq. (1) are widely used for many different quantum dissipative systems.[1] Our numerical algorithm can be applied to any of these systems as long as $J(\omega)$ is of superohmic type. However, in order to make closer contact to the existing literature on quantum dot dynamics we want to be more specific and employ a model which is widely used for the analysis of InGaAs self-assembled QDs. It is based on the following further assumptions: (a) the lattice properties of a confined QD do not differ significantly from the environment, so that one can describe the phonons as in the bulk material, where $\mathbf{q}$ denotes the phonon wave vector; (b) the carrier-phonon interaction is dominated by the deformation potential coupling with longitudinal acoustic phonons; (c) small frequency phonons are most important such that the dispersion can be taken to be linear, $\omega_{\mathbf{q}} = v_s|\mathbf{q}|$, where v_s is the sound velocity. From these assumptions we obtain

$$\gamma_{\mathbf{q}}^{e(h)} = \Psi^{e(h)}(\mathbf{q})\frac{|\mathbf{q}|D_{e(h)}}{\sqrt{2V\rho\hbar\omega_{\mathbf{q}}}}, \quad (3)$$

where ρ is the density of the material, V denotes the sample volume, $D_{e(h)}$ is the deformation potential constant, and $\Psi^{e(h)}(\mathbf{q})$ is the form factor, that can be calculated from the wave functions $\psi_{e(h)}(\mathbf{r})$ of the carriers confined in the QD as

$$\Psi^{e(h)}(\mathbf{q}) = \int_V |\psi_{e(h)}(\mathbf{r})|^2 \exp(i\mathbf{r}\mathbf{q}) d^3r. \quad (4)$$

Details of the wave functions are often not important. For simplicity we assume a spherical dot with wave functions

given by the ground-state solution of a harmonic potential, which gives

$$\Psi^{e(h)}(\mathbf{q}) = \exp\left(-\mathbf{q}^2 a_{e(h)}^2/4\right), \tag{5}$$

where a_e and a_h represent the electron and hole geometrical confinement lengths, respectively. Inserting Eqs. (3)–(5) into Eq. (2) we obtain

$$J(\omega) = \frac{\omega^3}{4\pi^2\rho\hbar v_c^5}\left\{D_e \exp\left(-\frac{\omega^2 a_e^2}{4v_c^2}\right) - D_h \exp\left(-\frac{\omega^2 a_h^2}{4v_c^2}\right)\right\}^2, \tag{6}$$

which scales for small frequencies as $J(\omega) \sim \omega^3$ and thus is indeed of superohmic type. Note that in the opposite limit of high frequencies $J(\omega)$ tends to zero as a Gaussian function, i.e., faster than usually assumed in studies of dissipative systems.

Finally we note, that other types of phonon modes or dispersions, e.g., half-space or slab modes,[27] can easily be handled by our approach as long as the modes form a continuum which results into a finite memory time.

III. PATH INTEGRALS FOR DOT DYNAMICS

A. Discretized path integrals

The time evolution of the statistical operator $\widehat{\rho}(t)$ of the total system, i.e., the QD and its environment, can be obtained from the Liouville–von Neumann equation

$$i\hbar\frac{d\widehat{\rho}}{dt} = [\widehat{H}, \widehat{\rho}]. \tag{7}$$

As usual we assume that the statistical operator initially is a product of carrier and phonon operators,

$$\widehat{\rho}(0) = \widehat{\overline{\rho}}(0) \otimes \frac{1}{Z}\exp\left(-\frac{1}{k_B T}\sum_{\mathbf{q}}\hbar\omega_{\mathbf{q}} b_{\mathbf{q}}^\dagger b_{\mathbf{q}}\right), \tag{8}$$

where Z is the normalization constant of the phonon distribution at temperature T, k_B is the Boltzmann constant, and $\widehat{\overline{\rho}}(0)$ is the initial statistical operator for the carrier subsystem. The solution of Eq. (7) together with the initial condition Eq. (8), traced over the phonon degrees of freedom, gives the dynamics of the reduced density matrix for the carrier states as

$$\widehat{\overline{\rho}}(t) = \mathrm{Tr}_{ph}[\widehat{U}(t)\widehat{\rho}(0)\widehat{U}^\dagger(t)], \tag{9}$$

where the time evolution operator is given by

$$\widehat{U}(t) = \widehat{T}\exp\left(\frac{i}{\hbar}\int_0^t \widehat{H}(t)dt\right), \tag{10}$$

and $\widehat{T}$ is the time ordering operator.

As shown in the Appendix, Eq. (9) can be written in the form of a path integral, where the trace over phonon variables is readily evaluated. For numerical calculations one needs a time discretized version of the functional integral with time intervals $\epsilon = t/N$, $t_n = \epsilon n$, where N is the total number of time slices. The discretized functional integral is defined in Eqs. (A32)–(A36) in the Appendix. Here we write the final expression for the reduced density matrix in the interaction picture, where the nondiagonal elements oscillate with the exciton transition frequency Ω and the frequency of the driving pulse is shifted to $\omega - \Omega$:

$$\overline{\rho}_{\alpha_N\beta_N} = e^{i\Omega t(\beta_N - \alpha_N)}\sum_{\{\alpha_n,\beta_n\}}\prod_{n=1}^{N} M_{\alpha_n}^{\alpha_{n-1}} M_{\beta_{n-1}}^{\beta_n *} \times \prod_{n'=1}^{n} e^{\mathcal{S}_{nn'}}\overline{\rho}_{\alpha_0\beta_0}(0). \tag{11}$$

The configuration summation in Eq. (11) is over all $\alpha_n, \beta_n = 0, 1$ with $n = 0, \ldots, N-1$ and $M_{\alpha_n}^{\alpha_{n-1}}$, $M_{\beta_{n-1}}^{\beta_n}$ are elements of the field transformation matrix M_n at the nth time step, which for small time steps, i.e., $\epsilon(\omega - \Omega) \ll 1$, reads

$$M_n = \begin{pmatrix} \cos f_n & -ie^{i(\Omega-\omega)t_n}\sin f_n \\ -ie^{-i(\Omega-\omega)t_n}\sin f_n & \cos f_n \end{pmatrix}, \qquad f_n = \frac{1}{2}\int_{t_{n-1}}^{t_n} f(t)dt.$$

The condition $\epsilon(\omega - \Omega) \ll 1$ for the validity of Eq. (IIIA) is always fulfilled at resonance $\Omega = \omega$ and is easy to fulfill close to resonance. In addition it should be noted that Eq. (IIIA) also becomes exact in the limit of ultrashort pulses, as shown in Eq. (A31).

The influence functional $S_{nn'}$ in Eq. (11) is given by

$$\mathcal{S}_{nn'} = -(\alpha_n - \beta_n)(K_{n-n'}\alpha_{n'} - K_{n-n'}^*\beta_{n'}), \tag{12}$$

where the phonon-induced memory kernel K_m, that accounts for influences that are retarded by m time steps, can be expressed in terms of the function

$$\Gamma(t) = \int_0^\infty d\omega J(\omega)\left[\cos(\omega t)\coth\left(\frac{\hbar\omega}{2k_B T}\right) - i\sin(\omega t)\right] \tag{13}$$

in the form

$$K_{m\neq 0} = \int_{m\epsilon}^{(m+1)\epsilon} d\tau\int_0^\epsilon d\tau'\Gamma(\tau - \tau') = 2\int_0^\infty d\omega\frac{J(\omega)}{\omega^2} \times [1 - \cos(\epsilon\omega)]\left\{\cos(\epsilon\omega m)\coth\left(\frac{\hbar\omega}{2k_B T}\right) - i\sin(\epsilon\omega m)\right\}, \tag{14}$$

$$K_{m=0} = \int_0^\epsilon d\tau\int_0^\tau d\tau'\Gamma(\tau - \tau') = \int_0^\infty d\omega\frac{J(\omega)}{\omega^2} \times \left\{[1 - \cos(\epsilon\omega)]\coth\left(\frac{\hbar\omega}{2k_B T}\right) - i\epsilon\omega + i\sin(\epsilon\omega)\right\}. \tag{15}$$

It is worth mentioning that the discrete form of the functional integral can also be obtained directly from the exact solution of Eq. (7) for the TLIB model in the case that the envelope function of a resonant excitation is a time equidistant sequence of δ pulses.[11,28]

B. Memory length truncation

An efficient method for the evaluation of the sums in Eq. (11) is obtained by introducing the so-called augmented

density matrix.[3,4] This procedure avoids the explicit summation of all terms, which is numerically prohibitive due to their large number (4^N for the two level system). It also bypasses usual difficulties of Monte Carlo methods that arise due to alternating signs in the discretized real-time path integrals. The augmented density matrix method requires that the memory kernel K_m tends sufficiently fast to zero for large m such that the memory can be truncated at a cutoff n_c ($K_{m>n_c} = 0$). The applicability of the method therefore depends on the long time asymptotics of the memory kernel and the related function $\Gamma(t)$ in Eq. (13).

At $T = 0\,\mathrm{K}$ the main term in the asymptotic expansion of $\Gamma(t)$ with the coupling from Eq. (6) is obtained as

$$\Gamma(t \to \infty) \to t^{-4}. \tag{16}$$

The imaginary part in this expansion is exponentially small, $\mathrm{Im}[\Gamma(t)] \propto \exp[-t^2/(2\tau_{ph}^2)]$, where τ_{ph} is the maximum of a_e/v_s and a_h/v_s, i.e., the time needed for a sound wave to cross the QD (typically of the order of a few ps). Equation (16) decays sufficiently fast to justify the truncation. At finite temperatures the real part of the asymptotic expansion acquires an additional temperature dependent term $\propto T \exp[-t^2/(2\tau_{ph}^2)]$. The relative weight of this additional term increases at higher temperatures becoming dominant when $k_B T \gtrsim \hbar/\tau_{ph}$. As the additional term decays exponentially the long time asymptotic is still given by the power law in Eq. (16). Nevertheless, the combination of both terms behaves like a system with an effectively shortened memory.

Further analysis of Eqs. (11)–(15) reveals that the important quantity that controls the dynamics of the system is

$$G(t = \epsilon m) = \sum_{n=1}^{m} \sum_{n'=1}^{n} K_{n-n'}, \tag{17}$$

which, according to Eqs. (14) and (15), reads as

$$G(t) = \int_0^t d\tau \int_0^\tau d\tau'\, \Gamma(\tau - \tau') = \int_0^\infty d\omega \frac{J(\omega)}{\omega^2} \times \left\{ [1 - \cos(\omega t)] \coth\left(\frac{\hbar\omega}{2k_B T}\right) - i[\omega t - \sin(\omega t)] \right\}. \tag{18}$$

Figure 1 displays the time dependence of K_m (where m has been taken as a continuous variable) and $G(t)$ at different temperatures. At $T = 0\,\mathrm{K}$ $G(t)$ becomes constant for times longer than 4.5 ps, while at higher temperatures of $T = 10\,\mathrm{K}$ or $T = 50\,\mathrm{K}$ the memory becomes shorter, taking values of roughly 3.5 ps.

The quantity $\exp[-G(t)]$ controls the time evolution of the nondiagonal density matrix element $\overline{\rho}_{01}$ after a single ultrashort pulse. It coincides with the exact solution of Eq. (7) for a single δ pulse excitation.[11] Taking again the coupling from Eq. (6) the long time asymptotic of Eq. (18) evaluates to

$$\begin{aligned} G(t \to \infty) &\to G_0 - i\Omega_p t, \\ G_0 &= \int_0^\infty \frac{J(\omega)}{\omega^2} \coth\left(\frac{\hbar\omega}{2k_B T}\right) d\omega = \text{const.}, \\ \Omega_p &= \int_0^\infty \frac{J(\omega)}{\omega} d\omega = \text{const.} \end{aligned} \tag{19}$$

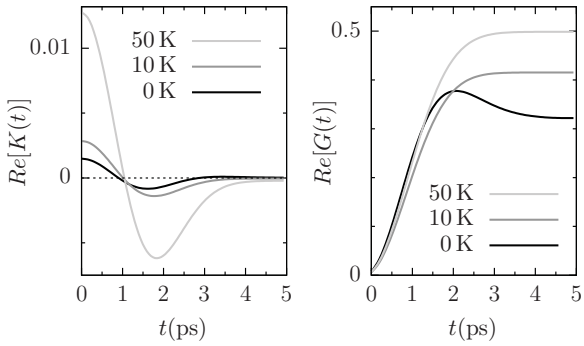

FIG. 1. Time dependence of the real part of the memory kernel $K(t)$ (left panel) and of the function $G(t)$ defined in Eq. (17) (right panel) for a $a_e = 5$ nm spherical InGaAs quantum dot with $a_h = 0.87\, a_e$ at different temperatures. For a better comparison, the values of $G(t)$ have been multiplied by a factor of 4 for $T = 10\,\mathrm{K}$ and by a factor of 10 for $T = 0\,\mathrm{K}$.

Here Ω_p is the standard polaronic shift, while G_0 defines the residual coherence that stays in the system in the long time limit (measured, e.g., as the asymptotic amplitude of the off-diagonal density matrix elements after a single δ pulse). At nonzero temperature G_0 increases with temperature, thereby reducing the residual coherence (cf. Fig. 1).

In order to obtain also within the truncation approximation, i.e., with $K^c_{m>n_c} = 0$, numerically an asymptotic behavior that is consistent with the exact solution for δ pulses, the asymptotic relations for the integral quantity $G(t)$ in Eqs. (17)–(19) must hold also for the truncated quantities. The long time asymptotic of $G(t)$ in Eq. (17) is obtained for the truncated memory kernel K^c_n as

$$\begin{aligned} G(t \to \infty) &\to G^c_0 + G^c_1 t, \\ G^c_0 = \sum_{n=1}^{n_c} \sum_{n'=1}^{n} K^c_{n-n'}, &\quad G^c_1 = \sum_{n=0}^{n_c} K^c_n. \end{aligned} \tag{20}$$

Comparing this with the exact asymptotic in Eq. (19) one obtains the following constraint for the truncated memory kernel:

$$\sum_{n=0}^{n_c} K^c_n = -i\epsilon\,\Omega_p, \tag{21}$$

which is consistent with the exact identity:

$$\sum_{n=0}^{\infty} K_n = \int_0^\infty \epsilon\,\Gamma(\tau) d\tau = -i \int_0^\infty \epsilon \frac{J(\omega)}{\omega} d\omega. \tag{22}$$

In the truncated memory approximation, it is most important to enforce this constraint for the real part of the kernel, i.e., to ensure that

$$\sum_{n=0}^{n_c} \mathrm{Re}\left[K^c_n\right] = 0. \tag{23}$$

It should be noted that the constraint Eq. (21) and the necessity of its enforcement is specific to the superohmic case. For the two-level system this can be most elegantly achieved by first noting that the polaronic shift Ω_p effectively leads to a renormalization of the transition frequency. It is

thus convenient to add it to the transition frequency, so that $\tilde{\Omega} = \Omega - \Omega_p$ replaces Ω in Eqs. (11) and (IIIA) and to remove the constant $-i\epsilon\Omega_p$ in Eq. (21) by modifying the kernel according to $\tilde{K}_0^c = K_0^c + i\epsilon\,\Omega_p$ and $\tilde{K}_n^c = K_n^c$ for $n > 0$. With this redefinition, Eq. (21) turns into

$$\sum_{n=0}^{n_c} \tilde{K}_n^c = 0, \tag{24}$$

which can be automatically fulfilled when we replace $\tilde{K}_n^c$ by

$$\bar{K}_n^c = \tilde{K}_n^c - \frac{1}{n_c+1}\sum_{n=0}^{n_c} \tilde{K}_n^c. \tag{25}$$

It should be noted that if Eq. (23) is not enforced the long time evolution of the system is dramatically altered by the truncation approximation since the time evolution of the off-diagonal density matrix elements acquires an additional exponential factor $\exp(-\mathrm{Re}[G_1^c]t)$. In this case Eq. (11) cannot reproduce known exact results. To demonstrate the importance of this constraint we show in Fig. 2 the polarization after a δ-like $\pi/2$ laser pulse for different temperatures. The simulations where Eq. (23) has been enforced by using Eq. (25) coincide exactly with known analytical results for ultrashort pulses. After a fast initial decay on a picosecond time scale we find a remnant polarization, the value of which depends strongly on the temperature. In contrast, simulations where this constraint has not been enforced show a qualitatively different behavior. Depending on the sign of $\mathrm{Re}[G_1^c]$ the long time behavior exhibits an additional exponential decay or even an increase. It should be noted that immediately after a $\pi/2$ pulse the modulus of the nondiagonal density matrix element reaches its maximal possible value, i.e., $|\overline{\rho}_{01}| = 1$. As the polarization is proportional to $|\overline{\rho}_{01}|$ it is therefore physically impossible that the polarization can rise from this starting point. Thus, values of $|P(t)/P(0)|^2$ above one that show up in Fig. 2 after ~ 15 ps in the zero temperature curve calculated without enforcing the constraint Eq. (23) are clearly unphysical.

It is instructive to analyze the consequences of the memory truncation on the time evolution in Eq. (11) for phonon couplings assumed to be either ohmic or subohmic, i.e., with a low-frequency scaling $J(\omega) \propto \omega^a$, with $a = 1$ (ohmic case)

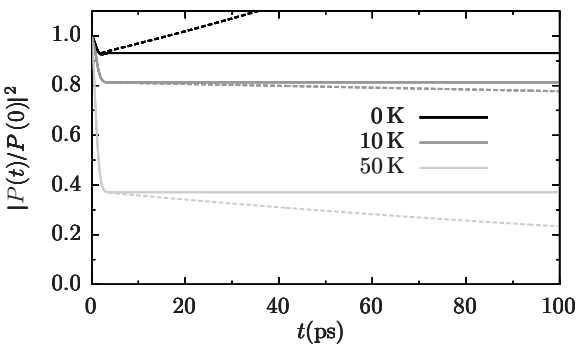

FIG. 2. Time dependence of the optical polarization induced by a δ-like $\pi/2$ pulse arriving at $t = 0$ ps at different temperatures. The solid lines correspond to numerical results obtained by enforcing Eq. (24) and are indistinguishable from analytically known exact results, while simulations without this constraint (dashed lines) show a qualitatively different long time behavior.

or with $0 \leqslant a < 1$ (subohmic case). The corresponding long time asymptotics are given by

$$\Gamma^{(a)}(t \to \infty) \to \gamma^{(a)} t^{-1-a}, \tag{26a}$$

$$G^{(a)}(t \to \infty) \to G^{(a)} t^{1-a} - i\Omega_p t, \tag{26b}$$

$$G^{(a=1)}(t \to \infty) \to G^{(a=1)} \ln t - i\Omega_p t, \tag{26c}$$

where $\gamma^{(a)}$ and $G^{(a)}$ are constants. Although $\Gamma^{(a)}(t)$ asymptotically decreases at long times for all $0 \leqslant a \leqslant 1$, an assumption of a finite memory length in the kernel K_n (and Γ) is not consistent with the $G^{(a)}(t)$ asymptotic in Eq. (26). Indeed, the asymptotic in Eq. (20) for the truncated memory kernel always leads to a linear time dependence, which according to Eq. (26) is found only for $a = 0$. Thus, for ohmic and subohmic coupling the finite memory approximation introduces qualitative changes in the long time behavior, and this can significantly affect the long time evolution of the system calculated according to Eq. (11). This contrasts to the case of superohmic coupling in QD systems for which the truncation cannot lead to qualitative changes of the system dynamics, if Eq. (21) holds. Possible quantitative errors due to the truncation can be well controlled by varying the time step and the memory truncation length.

Finally, we note that a similar truncation procedure must be followed when dealing with a multilevel system with superohmic couplings, as considered in the Appendix. However, for the case of different coupling constants one cannot introduce a single polaronic shift and, therefore, the constraint on the real parts in Eq. (23) must be enforced separately for all kernels $K_{\xi_n\zeta_{n'}}$ defined in Eq. (A35).

C. Numerical algorithm

The truncated memory length approximation enormously reduces the numerical load for the calculation of the reduced density matrix according to Eq. (11), or Eq. (A26) for the multilevel case, especially when it is combined with the so-called augmented density matrix formalism.[3,4] The original formulation of this method is somewhat cumbersome and required multiple runs of the algorithm to obtain the complete time evolution. Its subsequent improvement allowed an "on the fly" path selection, i.e., the most relevant paths are selected in the course of the time propagation in a single run. Here we present a brief summary of the method, adapted for the calculation of the QD dynamics.

To make the introduction of the algorithm most transparent we start from Eq. (11) to obtain the reduced density matrix at the time $t = t_n$ corresponding to the nth time slice with $n \leqslant N$:

$$\overline{\rho}_{\alpha_n\beta_n} = e^{-i\Omega t(\alpha_n-\beta_n)} \sum_{\{\alpha_{m<n},\beta_{m<n}\}} R_n(\{\alpha_m,\beta_m\}), \tag{27}$$

where R_n is a function of all variables $\{\alpha_m,\beta_m\}$ with $m = 0...n$ which is defined by the recurrence-like relation

$$R_n = T_n R_{n-1}, \tag{28a}$$

$$T_n = M_{\alpha_n}^{\alpha_{n-1}} M_{\beta_{n-1}}^{\beta_n *} \exp\left\{\sum_{n'=1}^{n} \mathcal{S}_{nn'}\right\}, \tag{28b}$$

$$R_0 = \overline{\rho}_{\alpha_0\beta_0}(0). \tag{28c}$$

This is not a true recurrence since R_{n-1} and R_n are functions of different numbers [$2n$ and $2(n+1)$] of the time slice variables $\{\alpha_m, \beta_m\}$. When the memory has a finite length, n_c, then T_n can be written as

$$T_n = M_{\alpha_n}^{\alpha_{n-1}} M_{\beta_{n-1}}^{\beta_n *} \exp\left\{ \sum_{n'=n-n_c}^{n} S_{nn'} \right\}, \tag{29}$$

which depends on $2(n_c+1)$ time slice variables. At step n T_n introduces connections between variables α_n, β_n and α_i, β_i in the time interval $n - n_c \leqslant i \leqslant n-1$, while the variables in the interval $0 \leqslant i \leqslant n - n_c - 1$ are not coupled. This allows us to sum R_n over the variables in the interval $0 \leqslant i \leqslant n - n_c - 1$, which introduces the *augmented density matrix* $\overline{R}_n$ as

$$\begin{aligned} \overline{R}_n &= \sum_{\alpha_0,\ldots,\alpha_{n-n_c-1}} \sum_{\beta_0,\ldots,\beta_{n-n_c-1}} R_n, \quad \text{at} \quad n > n_c, \\ \overline{R}_n &= R_n, \quad \text{at} \quad n \leqslant n_c. \end{aligned} \tag{30}$$

This implies that $\overline{R}_n$ depends on the same number of variables for all $n \geqslant n_c$. Using Eqs. (28) and (30) we obtain a true recurrence relation for $\overline{R}_{n>n_c}$ as

$$\overline{R}_n = \sum_{\alpha_{n-n_c-1}} \sum_{\beta_{n-n_c-1}} T_n \overline{R}_{n-1}, \tag{31}$$

while for $n \leqslant n_c$ Eq. (28) is used. The summation in Eq. (31) eliminates the dependence of $\overline{R}_n$ on the variables $\alpha_{n-n_c-1}, \beta_{n-n_c-1}$, while T_n adds the dependence on the variables α_n, β_n. Therefore, $\overline{R}_{n-1}$ and $\overline{R}_n$ depend on the same number of variables, or in other words $\overline{R}_{n-1}$ and $\overline{R}_n$ are objects of the same rank. Equation (31) is effectively a dynamical equation for the augmented density matrix, which in a sense does not have a memory as the matrix is fully defined by its values on the previous step. The price for a recurrence without memory is the increased dimensionality of the matrix. Figure 3 illustrates the structure of Eq. (31) for $n_c = 2$.

The reduced carrier density matrix at time step n, which is the real target of the calculation, is found from the augmented density matrix by summing over all those variables that correspond to times previous to t_n

$$\rho_{\alpha_n \beta_n} = e^{-i\Omega t(\alpha_n - \beta_n)} \sum_{\alpha_{n-1},\ldots,\alpha_{n-n_c}} \sum_{\beta_{n-1},\ldots,\beta_{n-n_c}} \overline{R}_n. \tag{32}$$

Writing the functional integral as a recurrence according to Eq. (31) reduces the number of required summations substantially. For $n \geqslant n_c$ we now have to account for 4^{n_c} configurations instead of 4^n which increases exponentially. Thus, the truncated memory approximation allows to calculate the time evolution for long times, if one can store and manipulate augmented density matrix tensors with a dimensionality of 4^{n_c}.

At a large memory length the efficiency of the method can be further improved, if one combines Eq. (31) with an "on-fly" path selection algorithm, similar to the one used in Ref. 5. To implement this selection algorithm it is convenient to represent the augmented density matrix $\overline{R}_{n-1}$ as a function of paths W_k, $k = 1, \ldots, k_{\max}$, where a path is a particular configuration of the variables $\{\alpha_m, \beta_m\}$ within the memory length, i.e., it is of the form $(\alpha_{n-1}, \ldots, \alpha_{n-n_c-1}, \beta_{n-1}, \ldots, \beta_{n-n_c-1})$. In the two-level system each path can thus be represented as a $2(n_c+1)$ long sequence of 0's and 1's. At times that exceed the memory length $n > n_c$ the algorithm can be described in three steps:

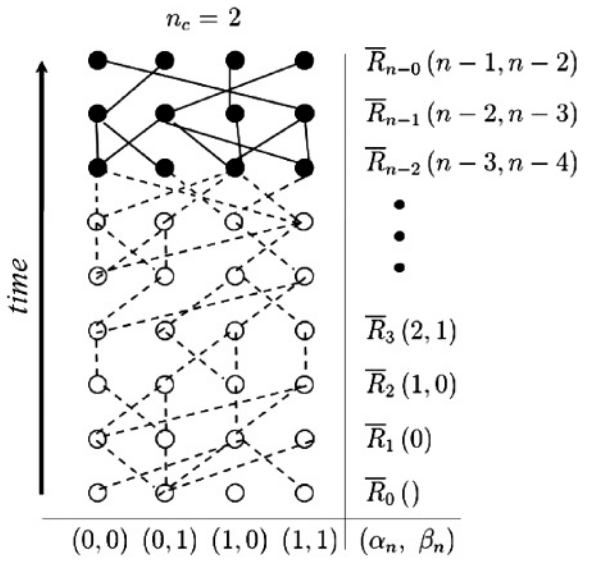

FIG. 3. Schematic representation of the truncation approximation for the recurrence sequence given in Eq. (30). The circles indicate time points t_n. Solid circles correspond to points within the memory length $n_c = 2$. Hollow circles are the time steps m with $n - m \geqslant n_c$, for which the corresponding paths have been summed out. The solid lines indicate the carrier paths included in $\overline{R}_n$, while the dashed lines indicate eliminated paths by summation.

1. We assume that at step $n-1$ we know all paths W_k, $k = 1, \ldots, k_{\max}$, of the length $2(n_c+1)$ that contribute noticeably to $\overline{R}_{n-1}$, i.e., paths that satisfy the condition $\overline{R}_{n-1}(W_k) > \delta$, where δ is a chosen threshold that sets the accuracy of the calculation.

2. We construct a product $R'_n = T_n \overline{R}_{n-1}(W_k)$ as in Eq. (31). By comparing all possible values of R'_n for all possible newly added variables $\alpha_n = 0,1$ and $\beta_n = 0,1$ we find all new noticeably contributing paths $\overline{W}_k$, $k = 1, \ldots, \overline{k}_{\max}$, of the form $(\alpha_n, \ldots, \alpha_{n-n_c-1}, \beta_n, \ldots, \beta_{n-n_c-1})$ that satisfy $R'_n(\overline{W}_k) > \delta$.

3. We sum those R'_n, that are relevant according to step 2, over the last variables $\alpha_{n-n_c-1}, \beta_{n-n_c-1}$ in the paths $\overline{W}_k$, as prescribed by Eq. (31). In the paths language this means the summation of R'_n for paths in which all values of $(\alpha_n, \ldots, \alpha_{n-n_c}, \beta_n, \ldots, \beta_{n-n_c})$ are the same. The summation procedure yields the augmented density matrix $\overline{R}_n$ at the next time step. At $n \leqslant n_c$ this step is omitted.

The procedure defined by steps 1–3 finds the most relevant paths by a recursive construction starting from some point. It is done "on the fly" and allows us to obtain the entire time evolution in a single run.

The accuracy of the numerical results depends on the time increment ϵ, the memory cutoff n_c, and the parameter δ to select the contributing paths. The maximal accuracy of the calculation is $O(\epsilon)$. However, a slight modification of the procedure[3,4] (setting $\epsilon/2$ time slices at both ends of the time interval) improves this accuracy to $O(\epsilon^2)$. The choice of the cutoff n_c is dictated by the effective temporal extension of the memory kernel, which follows from the dot geometry and the coupling mechanism. It can roughly be estimated

by τ_{ph}. The parameter δ can be fixed by comparing a few runs with different values until the results do not change with further decreasing δ. The choice of δ can be further checked by requiring that the calculation correctly reproduces cases, where exact solutions are known, e.g., the dynamics of a QD dot excited by a field with constant amplitude in the absence of phonons. A combination of n_c and δ determines the total number of paths that need to be stored in the computer memory. The large number of paths that need to be memorized is the main limitation of the algorithm, especially for models with larger numbers of carrier levels.

IV. NUMERICAL RESULTS

A few numerical applications of our implementation of the path integral approach to quantum dots have already been published without detailed explanation of the algorithm.[29,30] These studies revealed an interesting undamping effect of Rabi rotations at high-pulse areas. The corresponding calculations have been performed for the two-level model presented in Sec. II and rectangular pulse envelope functions $f(t)$. Of course, our algorithm is not restricted to rectangular pulses and can be used for pulses of any shape. This shall be illustrated here by simulations for Gaussian pulses that are more common in experiments. The results are in many respects qualitatively similar to those in Ref. 29. The remaining noticeable differences, in particular their physical origin, shall be analyzed in detail elsewhere. Here, we are mainly interested in the interrelation between changing physical excitation conditions and the efficiency and convergence properties of our algorithm.

To be specific we calculate the time evolution of the reduced electronic density matrix of a spherical tightly confined InGaAs QD with $a_e = 5$ nm and $a_h = 0.87\, a_e$ that is resonantly excited by a Gaussian pulse. The material parameters for the coupling between the dot and the longitudinal acoustic phonons are the same as in Ref. 11. It turns out that the results are converged for a time slice of $\epsilon = 0.4$ ps using a memory length of $n_c = 10$ and a path selecting parameter of $\delta = 10^{-9}$. A comparison with the plots in Fig. 1 shows that the memory kernel has practically vanished at the cut-off time $\epsilon\, n_c = 4.0$ ps. It is, however, surprising that the rather coarse grained time step of 0.4 ps is sufficient to achieve convergence. We have checked that taking finer time slices does indeed not change our results.

Figure 4 displays the time evolution of the occupation of the upper state, $\rho_{11}(t)$, for two representative temperatures of $T = 10$ K and 50 K at a total pulse area of $\alpha = 40\pi$. Clearly seen are decaying Rabi oscillations with a period that changes with time following the field intensity. The decay rate notably increases with temperature. However, the observation of Rabi oscillations in the time regime is often not convenient experimentally. Therefore, in many experiments the final occupation after the pulse is recorded as a function of the total pulse area α. Corresponding numerical results are plotted in Fig. 5 again for temperatures of $T = 10$ K and 50 K. The amplitude of the oscillations in Fig. 5 is a nonmonotonous function of the pulse area. For weak fields it decays with increasing field strength, while for strong fields it increases. This is the reappearance of Rabi rotations at high intensities

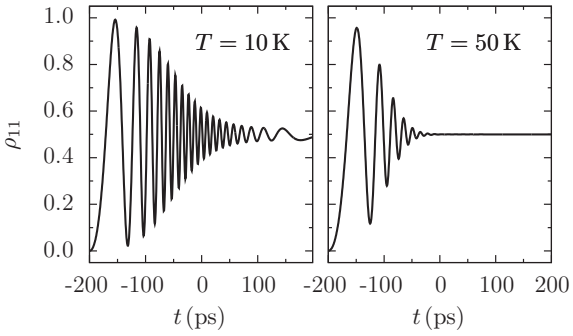

FIG. 4. Occupation ρ_{11} of the upper electronic state as a function of the time t for a Gaussian pulse with pulse area $\alpha = 40\pi$, pulse maximum at $t = 0$ and total duration of 140 ps (full width half maximum of the intensity) calculated for temperatures of $T = 10$ K and $T = 50$ K.

that has been discussed for rectangular pulses in Ref. 29. Despite some differences we conclude that the phenomenon is in essence also present for excitations with Gaussian pulses.

It is instructive to analyze how different physical excitation conditions affect the efficiency of our on-the-fly path selection algorithm. To this end, we performed calculations with and without path selection. Comparing results calculated with the on-the-fly algorithm for different values of the path selecting parameter δ with those, obtained by keeping all possible paths within the memory length, i.e., 4^{n_c}, reveals, how many paths have to be kept to achieve converged results. The black solid line in Fig. 6(a) shows as a function of the pulse area and for a fixed pulse duration of 18 ps (full-width half-maximum of the intensity) the fraction μ of all possible paths that has to be taken into account to achieve an error in ρ_{11} that is below 0.01. The corresponding path selecting parameter δ is plotted as a grey dotted line and shows a nonmonotonic behavior. Obviously, above $\alpha \sim 20\pi$ practically all paths have to be kept, and the on-the-fly selection algorithm is inefficient in highly nonlinear regimes. In contrast, below $\alpha \sim 5\pi$ less than 20% of the paths are relevant leading to a large speed-up of the numerics due to the path selection. In previous applications to ohmic systems without optical driving even higher efficiencies have been reported[5] with values of $\mu \leqslant 0.1\%$. Consistent with

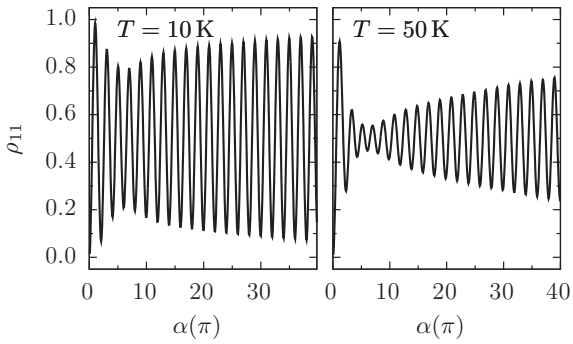

FIG. 5. Occupation ρ_{11} of the upper electronic state after excitation with a Gaussian pulse of 7 ps duration (full-width half-maximum of the intensity) as a function of the pulse area α calculated for temperatures of $T = 10$ K and $T = 50$ K.

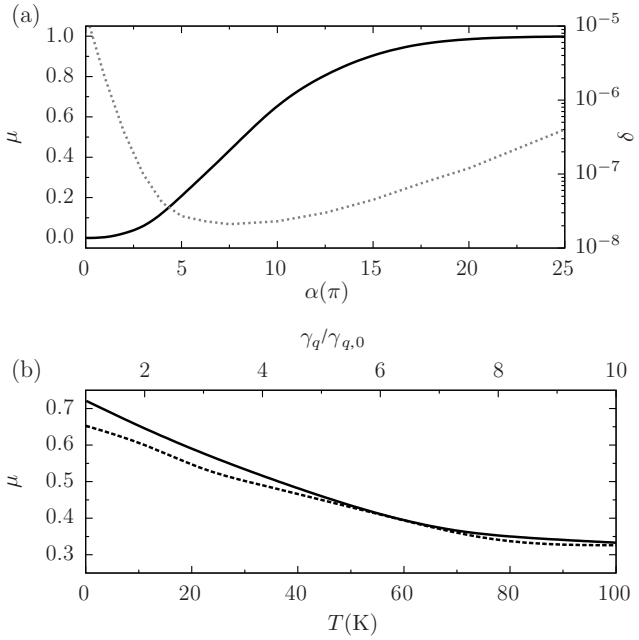

FIG. 6. Efficiency of the on-the-fly-algorithm. (a) fraction μ (black solid line) of all possible paths, that has to be taken into account to achieve an error in ρ_{11} below 0.01 as a function of the pulse area α at $T = 10\,\mathrm{K}$ for a Gaussian pulse of 18 ps duration. The grey dotted line displays the corresponding values of the path selection parameter δ. (b) shows the required fraction μ of all possible paths corresponding to an error smaller than 0.01 for a $10\,\pi$-pulse of 18 ps duration as a function of the temperature (solid, lower x axis) and as a function of the coupling constant γ_q at $T = 10\,\mathrm{K}$ (dashed, upper x axis). Here $\gamma_{q,0}$ is the coupling constant of GaAs, which has been used for all other plots shown in this work.

these findings, we obtain similar low values in the limit of vanishing pulse areas.

Besides the external driving, the temperature and the coupling strength significantly influence the efficiency of our algorithm. Shown in Fig. 6(b) is μ as a function of the temperature (solid, lower x axis) for $\alpha = 10\pi$ and a fixed pulse duration of 18 ps and also as a function of the carrier-phonon coupling strength (dashed, upper x axis) for the same pulse and at $T = 10\,\mathrm{K}$. In order to explore the dependence on the coupling strength we have scaled the $\gamma_{\mathbf{q}}$ values that correspond to our standard GaAs parameters by a factor indicated on the upper axis. It has been noted before[29] that increasing the temperature and increasing the carrier-phonon coupling act in many respects in similar ways on the system. This is also reflected in Fig. 6(b), where μ shows similar tendencies as a function of T and $\gamma_{\mathbf{q}}$. At low temperatures or weak couplings between 60 and 70% of the paths are relevant, while for temperatures above 80 K or couplings about 10 times stronger than in GaAs less than 35% are needed. We note that GaAs corresponds rather to the low-coupling limit. Effective couplings to acoustic phonons that are 10 times stronger are found, e.g., for the piezoelectric coupling in GaN.[31]

The efficiency of the path selection algorithm is primarily defined by the number of paths necessary for the accurate description of oscillating functions. Rabi oscillations of higher amplitude and frequency generally require a larger number of contributing paths. We have seen this already in discussing the decreased efficiency at higher Rabi frequencies, shown in Fig. 6(a). Now at increased temperatures the amplitude of the oscillations decays faster, as shown in Fig. 4, also leading to a decreased number of relevant paths. A similar decay of Rabi oscillations is observed at larger coupling strengths, resulting in a similar efficiency increase, shown in Fig. 6(b). An additional factor that may influence the number of paths is the effective memory length. It is affected by temperature, which generally shifts the relevant features of the memory kernel toward earlier times, as shown in Fig. 1. However, when scaling the coupling, as done in Fig. 6(b), the form of the memory kernel is not changed and thus the memory is not shortened. Therefore, a change of the memory length is not responsible for the reduction of required paths in this case.

V. CONCLUSION

We have presented a numerical real time path integral approach that is specially adapted to systems with superohmic system bath coupling. As a prototype for such a system we have considered a laser-driven strongly confined quantum dot coupled to acoustic phonons via the deformation potential coupling. Based on the augmented density matrix formalism, explicit formulas for the discretized propagation of the reduced electronic density matrix are given for two- and multilevel electronic models. In addition, it is described how this propagation scheme can be combined with an on-the-fly path selection method to further enhance the numerical efficiency. Our implementation accounts for arbitrary driving forces by external laser fields while previous studies with similar approaches have concentrated on initial value problems for cases with ohmic or subohmic couplings. We have demonstrated that for systems with superohmic coupling the propagation yields the correct asymptotic long time behavior when constraints, that hold exactly in the continuous formulation of the path integral, are enforced in the discretized form with a truncated memory that is used in the numerical implementation. In contrast, for systems with ohmic or subohmic coupling the memory truncation introduces qualitative changes of the long time asymptotics.

For a system driven by a sequence of ultrashort pulses the formulas provided by our discretized propagation scheme coincide with known exact analytical results for this case. For pulses of arbitrary shape the algorithm yields results with a well-controlled numerical error. As an illustration we have calculated the time evolution of a quantum dot system after excitation with a Gaussian pulse. Similar to previous studies with rectangular pulses we find a revival of Rabi rotations at high pulse areas. Our studies also reveal a strong dependence of the efficiency of the on-the-fly path selection on physical excitation conditions. The algorithm turns out to be highly efficient only for not too strong laser-induced nonlinearities. Interestingly, the efficiency of the path selection rises considerably for high temperatures and strong carrier-phonon couplings. We believe that the method developed in this paper will pave the way toward many new studies of quantum dissipative systems with superohmic coupling, in particular quantum dots, in regimes that have so far been out of reach with other methods. This includes highly nonlinear

dynamics as well as high-temperature and/or strong-coupling scenarios.

ACKNOWLEDGMENTS

M.D.C. is grateful for the support of the Alexander von Humboldt Foundation.

APPENDIX: DISCRETIZED PATH INTEGRALS FOR MULTILEVEL SYSTEMS

In this appendix we derive a discretized path integral representation of the dynamics for a laser-driven multilevel carrier system that is coupled to acoustic phonons by pure-dephasing type interactions. The derivation relies on the linear carrier-phonon coupling, which allows to eliminate the phonon related degrees of freedom exactly and to construct an effective Feynman-Vernon–like functional for the carrier states. Although this type of procedure is well established in the literature there are several reasons why it is worth presenting here. Most derivations concentrate on the two-level case and explicit formulas for the multiple level case are rarely found. Finally, details of the numerical procedure are strongly connected with the derivation of the path integral itself and therefore, presenting the derivation will make these procedures more transparent.

We shall focus on a quantum dot system described by the following generic Hamiltonian:

$$\begin{aligned} \widehat{H} &= \widehat{H}_0 + \widehat{H}_1, \quad \widehat{H}_0 = \hbar\widehat{\Omega} + \hbar\widehat{M}(t), \\ \widehat{H}_1 &= \hbar\sum_{\mathbf{q}} (\widehat{\gamma}_{\mathbf{q}} b_{\mathbf{q}}^{+} + \widehat{\gamma}_{\mathbf{q}}^{*} b_{\mathbf{q}}) + \hbar\sum_{\mathbf{q}} \omega_{\mathbf{q}} b_{\mathbf{q}}^{\dagger} b_{\mathbf{q}}, \end{aligned} \tag{A1}$$

where the hat sign stands for matrix operators, acting in the space of carrier states, $\hbar\widehat{\Omega}$ is a diagonal matrix with the energies of the states on the diagonal, $\widehat{M}(t)$ describes transitions between the carrier states induced by the coupling with external light, and $\widehat{\gamma}_{\mathbf{q}}$ is a diagonal matrix accounting for the coupling of phonons to the different electronic levels.

The dynamics of the system is given by the Liouville–von Neumann equation. From its solution the dynamics of the reduced carrier density matrix is obtained according to Eq. (9). Thus, the path integral representation for the reduced carrier density matrix follows from that for the evolution operator given by Eq. (10). The latter is obtained by following several standard steps. First, the evolution operator which corresponds to the Hamiltonian in Eq. (A1) is discretized using the Trotter formula,

$$\widehat{U}(t) = \lim_{N\to\infty} \prod_{n=1}^{N} e^{-i\epsilon \widehat{H}(t_n)/\hbar}, \tag{A2}$$

where $t_n = \epsilon n$, $t_0 = 0$, $t_N = t$, and the product is time ordered, with decreasing n from left to right. For numerical calculations one approximates Eq. (A2) with finite N and ϵ. The product in Eq. (A2) is converted into a summation over a multidimensional configuration space by inserting identity operators $\widehat{I}_n$ as

$$\widehat{U}(t) \approx e^{-i\epsilon \widehat{H}(t_N)/\hbar} \widehat{I}_{N-1}, \ldots, \widehat{I}_1 e^{-i\epsilon \widehat{H}(t_1)/\hbar}. \tag{A3}$$

Each of the identity operators $\widehat{I}_n$ is constructed as a direct product of identity operators in the space of carrier states, $|\alpha_n\rangle$, and coherent phonon states, $|\mathcal{Z}_n\rangle$, defined by $b_{\mathbf{q}}|\mathcal{Z}_n\rangle = z_{\mathbf{q}n}|\mathcal{Z}_n\rangle$, so that

$$\begin{aligned} \widehat{I}_n = \widehat{I}_n^{\alpha} \otimes \widehat{I}_n^{z}, \quad \widehat{I}_n^{\alpha} = \sum_{\alpha_n} |\alpha_n\rangle\langle\alpha_n|, \quad \widehat{I}_n^{z} = \int d\mu_n |\mathcal{Z}_n\rangle\langle\mathcal{Z}_n|, \\ d\mu_n = \prod_{\mathbf{q}} e^{-\bar{z}_{\mathbf{q}n} z_{\mathbf{q}n}} \frac{d\bar{z}_{\mathbf{q}n} dz_{\mathbf{q}n}}{\pi}, \end{aligned} \tag{A4}$$

where the integration is done on the complex plane of the conjugate variables $z_{\mathbf{q}n}$ and $\bar{z}_{\mathbf{q}n} = z_{\mathbf{q}n}^{*}$. In this representation the matrix elements of the evolution operator in Eq. (A3) read as

$$\begin{aligned} &\langle \alpha_N, \mathcal{Z}_N | \widehat{U}(t) | \alpha_0, \mathcal{Z}_0 \rangle \\ &\quad = \sum_{\alpha_1} \cdots \sum_{\alpha_{N-1}} \int d\mu_1 \cdots \int d\mu_{N-1}\, U_N\, U_{N-1} \cdots U_1, \\ &\quad U_n = \langle \alpha_n, \mathcal{Z}_n | e^{-i\epsilon \widehat{H}(t_n)/\hbar} | \alpha_{n-1}, \mathcal{Z}_{n-1} \rangle. \end{aligned} \tag{A5}$$

Keeping the accuracy of the discretization $O(\epsilon)$, the operator exponent in Eq. (A2) can be written as

$$e^{-i\epsilon \widehat{H}(t_n)/\hbar} \approx e^{-i\epsilon \widehat{H}_1(t_n)/\hbar} e^{-i\epsilon \widehat{H}_0(t_n)/\hbar}, \tag{A6}$$

and the matrix element U_n reads

$$\begin{aligned} U_n = \langle \mathcal{Z}_n, \alpha_n | e^{-i\epsilon \widehat{H}_1(t_n)/\hbar} | \mathcal{Z}_{n-1}, \alpha_n \rangle \\ \langle \alpha_n | e^{-i\epsilon \widehat{H}_0(t_n)/\hbar} | \alpha_{n-1} \rangle, \end{aligned} \tag{A7}$$

where we have used the fact that $\widehat{H}_0$ is diagonal in the phonon sub space and that $\widehat{H}_1$ is diagonal in the subspace of carrier states. Using a standard result for matrix elements of a normal-ordered phonon operator function,

$$\langle \mathcal{Z} | F(b_{\mathbf{q}}^{\dagger}, b_{\mathbf{q}}) | \mathcal{Z}' \rangle = e^{\sum_{\mathbf{q}} \bar{z}_{\mathbf{q}} z'_{\mathbf{q}}} F(\bar{z}_{\mathbf{q}}, z'_{\mathbf{q}}), \tag{A8}$$

and again keeping the accuracy $O(\epsilon)$ we evaluate the first matrix element in Eq. (A7) as

$$\langle \mathcal{Z}_n, \alpha_n | e^{-i\epsilon \widehat{H}_1/\hbar} | \mathcal{Z}_{n-1}, \alpha_n \rangle \approx \langle \alpha_n | e^{\widehat{S}_n} | \alpha_n \rangle, \tag{A9}$$

where

$$\begin{aligned} \widehat{S}_n = \sum_{\mathbf{q}} \bar{z}_{\mathbf{q}n} z_{\mathbf{q}n-1} - i\epsilon \sum_{\mathbf{q}} (\widehat{\gamma}_{\mathbf{q}n} \bar{z}_{\mathbf{q}n} + \widehat{\gamma}_{\mathbf{q}n}^{*} z_{\mathbf{q}n-1}) \\ - i\epsilon \sum_{\mathbf{q}} \omega_{\mathbf{q}} \bar{z}_{\mathbf{q}n} z_{\mathbf{q}n-1}. \end{aligned} \tag{A10}$$

The index n in the matrix $\widehat{\gamma}_{\mathbf{q}n}$ is introduced to stress that it acts on carrier states of the nth time slice.

In the limit ($N \to \infty, \epsilon \to 0, N\epsilon = t$) the matrix elements of the evolution operator, defined in Eqs. (A5)–(A10), become a path integral over phonon variables, formally written as

$$\langle \mathcal{Z}_f, \alpha_f | \widehat{U}(t) | \mathcal{Z}_i, \alpha_i \rangle = \langle \alpha_f | \int \mathcal{D}\mathcal{Z} \widehat{\mathrm{T}}[e^{\widehat{S}}] | \alpha_i \rangle, \tag{A11}$$

where initial and final states are denoted by indices $i(n = 0)$ and $f(n = N)$. $\widehat{\mathrm{T}}$ is the time ordering operator for the operators

in the carrier state space and the "action" $\widehat{S}$ is also an operator in the same space given by

$$\widehat{S} = \sum_{\mathbf{q}} \bar{z}_{\mathbf{q}}(t) z_{\mathbf{q}}(t) - \frac{i}{\hbar}\int_0^t \widehat{H}_0(\tau)d\tau - \int_0^t d\tau \sum_{\mathbf{q}} [\bar{z}_{\mathbf{q}}(\tau)\dot{z}_{\mathbf{q}}(\tau) + i\omega_{\mathbf{q}}\bar{z}_{\mathbf{q}}(\tau)z_{\mathbf{q}}(\tau) + i\widehat{\gamma}_{\mathbf{q}}(\tau)\bar{z}_{\mathbf{q}}(\tau) + i\widehat{\gamma}_{\mathbf{q}}(\tau)^* z_{\mathbf{q}}(\tau)]. \tag{A12}$$

In deriving Eq. (A12) we have used the identity

$$\sum_{n=1}^{N} \bar{z}_{\mathbf{q}n} z_{\mathbf{q}n-1} - \sum_{n=1}^{N-1} \bar{z}_{\mathbf{q}n} z_{\mathbf{q}n} = \bar{z}_{\mathbf{q}N} z_{\mathbf{q}N} - \epsilon \sum_{n=1}^{N} \bar{z}_{\mathbf{q}n} \frac{z_{\mathbf{q}n} - z_{\mathbf{q}n-1}}{\epsilon}. \tag{A13}$$

The definition of the path integral is complete with the boundary conditions

$$z_{\mathbf{q}}(0) = z_{\mathbf{q}i}, \quad \bar{z}_{\mathbf{q}}(t) = z^*_{\mathbf{q}f}. \tag{A14}$$

The matrix elements of the statistical operator are obtained by performing the matrix products in Eq. (9) in the chosen representation for the phonon and carrier states. The reduced carrier density matrix then follows after taking the trace over the phonon degrees of freedom. Here this is equivalent to integrations over the phonon variables $z_{\mathbf{q}f}$ as

$$\widehat{\bar{\rho}}_{\alpha_f,\beta_f}(t) = \sum_{\alpha_i,\beta_i} \int d\mu_f d\mu_i d\mu_i' \langle \mathcal{Z}_f,\alpha_f|\widehat{U}(t)|\mathcal{Z}_i,\alpha_i\rangle \times \langle \mathcal{Z}_i,\alpha_i|\widehat{\rho}(0)|\mathcal{Z}_i',\beta_i\rangle\langle \mathcal{Z}_i',\beta_i|\widehat{U}^\dagger(t)|\mathcal{Z}_f,\beta_f\rangle, \tag{A15}$$

where the matrix elements of the operator $\widehat{U}^\dagger(t)$ read

$$\langle \mathcal{Z}_i',\beta_i|\widehat{U}^\dagger(t)|\mathcal{Z}_f,\beta_f\rangle = \langle\beta_i|\int \mathcal{D}\mathcal{Z}'\widehat{\mathrm{T}}[e^{\widehat{S}'}]|\beta_f\rangle, \tag{A16}$$

with

$$\widehat{S}' = \sum_{\mathbf{q}} \bar{z}'_{\mathbf{q}}(t) z'_{\mathbf{q}}(t) + \frac{i}{\hbar}\int_0^t \widehat{H}_0'(\tau)d\tau - \int_0^t d\tau \sum_{\mathbf{q}} \left[z'_{\mathbf{q}}(\tau)\dot{\bar{z}}'_{\mathbf{q}}(\tau) - i\omega_{\mathbf{q}}\bar{z}'_{\mathbf{q}}(\tau)z'_{\mathbf{q}}(\tau) - i\widehat{\gamma}'_{\mathbf{q}}\bar{z}'_{\mathbf{q}}(\tau) - i\widehat{\gamma}'^*_{\mathbf{q}} z'_{\mathbf{q}}(\tau)\right]. \tag{A17}$$

The trajectories in Eq. (A17) satisfy the boundary conditions

$$z'_{\mathbf{q}}(t) = z_{\mathbf{q}f}, \quad \bar{z}'_{\mathbf{q}}(0) = z'^*_{\mathbf{q}i}. \tag{A18}$$

The initial statistical operator $\widehat{\rho}(0)$ is defined by Eq. (8), which in the phonon coherent states representation assumes the form

$$\langle \mathcal{Z}_i,\alpha_i|\widehat{\rho}(0)|\mathcal{Z}_i',\beta_i\rangle = \frac{1}{Z}\exp\left[\sum_{\mathbf{q}} e^{-\frac{\hbar\omega_{\mathbf{q}}}{k_B T}} z^*_{\mathbf{q}i} z'_{\mathbf{q}i}\right]\widehat{\bar{\rho}}_{\alpha_i\beta_i}(0). \tag{A19}$$

Since the action in Eqs. (A12) and (A17) is quadratic in the phonon variables the corresponding path integrals can be calculated analytically. This can be done either in the discretized representation defined in Eqs. (A5)–(A10) or, alternatively, in the continuous formulation given in Eqs. (A11)–(A14) and (A16)–(A18). In the latter approach the path integral for the evolution operator is defined by the "classical" trajectories, found from the condition of extremal action, so that

$$\langle \mathcal{Z}_f,\alpha_f|\widehat{U}(t)|\mathcal{Z}_i,\alpha_i\rangle \propto \langle\alpha_f|\exp(\widehat{S}_{\mathrm{cl}})|\alpha_i\rangle, \tag{A20}$$

where $\widehat{S}_{\mathrm{cl}}$ is the extremal action. Accounting for deviations from those trajectories yields a nonessential time dependent factor, which is absorbed by a normalization, when the result is substituted to calculate the final density matrix. The trajectories for the extremal action are determined by the equations

$$\frac{\partial S}{\partial \bar{z}_{\mathbf{q}}} = \dot{z}_{\mathbf{q}} + i\omega_{\mathbf{q}} z_{\mathbf{q}} + i\widehat{\gamma}_{\mathbf{q}} = 0, \quad \frac{\partial S}{\partial z_{\mathbf{q}}} = \dot{\bar{z}}_{\mathbf{q}} - i\omega_{\mathbf{q}}\bar{z}_{\mathbf{q}} - i\widehat{\gamma}^*_{\mathbf{q}} = 0, \tag{A21}$$

that are complemented with the boundary conditions in Eq. (A14). The corresponding solutions are

$$z_{\mathbf{q}}(\tau) = e^{-i\omega_{\mathbf{q}}\tau} z_{\mathbf{q}i} - i\int_0^\tau e^{-i\omega_{\mathbf{q}}(\tau-\tau')}\widehat{\gamma}_{\mathbf{q}}(\tau')d\tau', \quad \bar{z}_{\mathbf{q}}(\tau) = e^{i\omega_{\mathbf{q}}(\tau-t)} z^*_{\mathbf{q}f} - i\int_\tau^t e^{i\omega_{\mathbf{q}}(\tau-\tau')}\widehat{\gamma}^*_{\mathbf{q}}(\tau')d\tau'. \tag{A22}$$

We note, that these solutions are operators in the carrier state space. Also, it is easily seen, that now they are not complex conjugate which justifies the notation $\bar{z}$.

The extremal action $\widehat{S}_{\mathrm{cl}}$ is obtained by substituting Eq. (A22) into Eq. (A12), which yields

$$\widehat{S}_{\mathrm{cl}}(t) = -\frac{i}{\hbar}\int_0^t \widehat{H}_0(\tau)d\tau + \sum_{\mathbf{q}} z^*_{\mathbf{q}f} z_{\mathbf{q}i} e^{-i\omega_{\mathbf{q}}t} - \sum_{\mathbf{q}}\int_0^t d\tau \int_0^\tau d\tau' e^{i\omega_{\mathbf{q}}(\tau'-\tau)}\widehat{\gamma}^*_{\mathbf{q}}(\tau)\widehat{\gamma}_{\mathbf{q}}(\tau') - i\sum_{\mathbf{q}} z^*_{\mathbf{q}f}\int_0^t e^{i\omega_{\mathbf{q}}(\tau-t)}\widehat{\gamma}_{\mathbf{q}}(\tau)d\tau - i\sum_{\mathbf{q}} z_{\mathbf{q}i}\int_0^t e^{-i\omega_{\mathbf{q}}\tau}\widehat{\gamma}^*_{\mathbf{q}}(\tau)d\tau. \tag{A23}$$

For the path integral in Eq. (A16) the extremal action is found along the same lines as

$$\widehat{S}'_{\mathrm{cl}}(t) = \frac{i}{\hbar}\int_0^t \widehat{H}_0'(\tau)d\tau + \sum_{\mathbf{q}} z_{\mathbf{q}f} z'^*_{\mathbf{q}i} e^{i\omega_{\mathbf{q}}t} - \sum_{\mathbf{q}}\int_0^t d\tau \int_0^\tau d\tau' e^{-i\omega_{\mathbf{q}}(\tau'-\tau)}\widehat{\gamma}'_{\mathbf{q}}(\tau)\widehat{\gamma}'^*_{\mathbf{q}}(\tau') + i\sum_{\mathbf{q}} z_{\mathbf{q}f}\int_0^t e^{-i\omega_{\mathbf{q}}(\tau-t)}\widehat{\gamma}'^*_{\mathbf{q}}(\tau)d\tau + i\sum_{\mathbf{q}} z'^*_{\mathbf{q}i}\int_0^t e^{i\omega_{\mathbf{q}}\tau}\widehat{\gamma}'_{\mathbf{q}}(\tau)d\tau. \tag{A24}$$

Both $\widehat{S}$ and $\widehat{S}'$ in Eqs. (A23) and (A24) are operators in the space of carriers states, denoted by indices α and β for $\widehat{S}$

and $\widehat{S}'$, respectively. Substituting Eqs. (A23) and (A24) into Eq. (A15) we obtain the reduced carrier density matrix as

$$\widehat{\widehat{\rho}}_{\alpha_f,\beta_f}(t) = \sum_{\alpha_i,\beta_i} \int d\mu_f d\mu_i d\mu_i' \langle \alpha_f,\beta_f|\widehat{T}\widehat{T}' e^{\widehat{S}_{\rm cl}+\widehat{S}_{\rm cl}'}|\alpha_i,\beta_i\rangle \times \exp\left(\sum_{\mathbf{q}} e^{-\frac{\hbar\omega_{\mathbf{q}}}{k_B T}} z_{\mathbf{q}i}^* z_{\mathbf{q}i}'\right) \widehat{\widehat{\rho}}_{\alpha_i,\beta_i}(0). \tag{A25}$$

After integration over $z_{\mathbf{q}i}$, $z_{\mathbf{q}f}$, and $z_{\mathbf{q}i}'$ one obtains finally

$$\widehat{\widehat{\rho}}_{\alpha_f\beta_f}(t) = \sum_{\alpha_i,\beta_i} \langle \alpha_f,\beta_f|\widehat{T}\widehat{T}' e^{\widehat{S}_0+\widehat{S}_{\rm inf}}|\alpha_i,\beta_i\rangle \widehat{\widehat{\rho}}_{\alpha_i\beta_i}(0), \tag{A26}$$

where

$$\widehat{S}_0 = -i\int_0^t [\widehat{M}(\tau) - \widehat{M}'(\tau)]d\tau \tag{A27}$$

describes field-induced rotations in the carrier state space and the influence functional $\widehat{S}_{\rm inf}$ is given by

$$\widehat{S}_{\rm inf} = -i(\widehat{\Omega}-\widehat{\Omega}')t - \sum_{\mathbf{q}} \Bigg\{ n_{\mathbf{q}} \int_0^t d\tau e^{-i\omega_{\mathbf{q}}\tau}[\widehat{\gamma}_{\mathbf{q}}^*(\tau) - \widehat{\gamma}_{\mathbf{q}}'^*(\tau)] \times \int_0^t d\tau' e^{i\omega_{\mathbf{q}}\tau'}[\widehat{\gamma}_{\mathbf{q}}(\tau') - \widehat{\gamma}_{\mathbf{q}}'(\tau')] - \int_0^t d\tau \int_0^t d\tau' e^{i\omega_{\mathbf{q}}(\tau-\tau')} \times \widehat{\gamma}_{\mathbf{q}}(\tau)\widehat{\gamma}_{\mathbf{q}}'^*(\tau') + \int_0^t d\tau \int_0^\tau d\tau' [e^{-i\omega_{\mathbf{q}}(\tau-\tau')}\widehat{\gamma}_{\mathbf{q}}^*(\tau)\widehat{\gamma}_{\mathbf{q}}(\tau') + e^{i\omega_{\mathbf{q}}(\tau-\tau')}\widehat{\gamma}_{\mathbf{q}}'(\tau)\widehat{\gamma}_{\mathbf{q}}'^*(\tau')] \Bigg\}, \tag{A28}$$

where $n_{\mathbf{q}} = [\exp(\hbar\omega_{\mathbf{q}}/k_B T) - 1)]^{-1}$. Equation (A28) can be written in a simpler form, when the coupling constants satisfy certain symmetry conditions. For example, when all $\gamma_{\mathbf{q}\alpha}$ are purely real or imaginary, or the system contains only two carrier states and $\gamma_{\mathbf{q}0} = 0$, then Eq. (A28) can be written as

$$\widehat{S}_{\rm inf} = -i(\widehat{\Omega} - \widehat{\Omega}')t - \sum_{\mathbf{q}} \int_0^t d\tau \int_0^\tau d\tau' [\widehat{\gamma}_{\mathbf{q}}^*(\tau) - \widehat{\gamma}_{\mathbf{q}}'^*(\tau)] \times [\eta_{\mathbf{q}}(\tau-\tau')\widehat{\gamma}_{\mathbf{q}}(\tau') - \eta_{\mathbf{q}}^*(\tau-\tau')\widehat{\gamma}_{\mathbf{q}}'(\tau')], \tag{A29}$$

where we have introduced the notation

$$\eta_{\mathbf{q}}(\tau) = \coth\left(\frac{\hbar\omega_{\mathbf{q}}}{2k_B T}\right)\cos(\omega_{\mathbf{q}}\tau) - i\sin(\omega_{\mathbf{q}}\tau). \tag{A30}$$

Equations (A26)–(A30) define the path integral expressed using continuous time ordered products of operators in the carrier state space. In order to develop a numerical algorithm for practical calculations we shall return to a suitable discretized representation. Since the main steps in this procedure are analogous to the construction of the original path integral with phonon variables, we only highlight the essential differences.

As before we use Eq. (A2), with finite time slices ϵ. The identity operators are then inserted as in Eq. (A3). As the system is now described by two sets of carrier states, $|\alpha_n\rangle$ and $|\beta_n\rangle$, for the forward and for the backward time propagation, respectively, the identity operators are a direct product $\widehat{I}_n = \widehat{I}_n^\alpha \otimes \widehat{I}_n^\beta$. In order to calculate matrix elements of the operator exponents between states at time slices n and $n-1$ we approximate the matrix exponent as in Eq. (A6). The first part contains the influence functional $\widehat{S}_{\rm inf}$, that has only diagonal phonon coupling matrices, while the second part contains $\widehat{S}_0$, with nondiagonal operators in the carrier state space.

Here, integrals of $\widehat{S}_{\rm inf}$ and $\widehat{S}_0$ over the time slices appear in the exponents, not their first order approximation as in Eq. (A6). This yields a considerable improvement of the accuracy for the diagonal part $\widehat{S}_{\rm inf}$, which yields an exact solution in the absence of the external driving. It is easy to see that this discretization scheme for the path integral in fact gives the exact solution in the case when the external driving is given by a sequence of delta pulses arriving at times $t_n = \epsilon n$:

$$\widehat{M}(t) = \epsilon \sum_{n=1}^{N} \widehat{M}(t_n)\delta(t - \epsilon n). \tag{A31}$$

When the influence functional reduces to the form in Eq. (A29) the discretized version of Eq. (A26) becomes

$$\widehat{\widehat{\rho}}_{\alpha_N\beta_N} = \sum_{\{\alpha_n,\beta_n\}} \Bigg\{ \prod_{n=1}^{N} M_{\alpha_n}^{\alpha_{n-1}} M_{\beta_{n-1}}^{\beta_n *} e^{-i(\Omega_{\alpha_n}-\Omega_{\beta_n})\epsilon} \times \prod_{n'=1}^{n} e^{\mathcal{S}_{nn'}} \widehat{\widehat{\rho}}_{\alpha_0\beta_0} \Bigg\}, \tag{A32}$$

where the configuration summation is over all $\alpha_n, \beta_n = 0, 1$ with $n = 0, \ldots, N-1$ and matrices M describe external field influences and are defined as

$$M_{\alpha_n}^{\alpha_{n-1}} = \langle \alpha_n | e^{-i\epsilon \widehat{M}(t_n)} | \alpha_{n-1}\rangle, \tag{A33}$$

while the discretized form of the influence functional is

$$\mathcal{S}_{nn'} = -K_{\alpha_{n'}\alpha_n} - K_{\beta_n\beta_{n'}}^* + K_{\alpha_n\beta_{n'}}^* + K_{\alpha_{n'}\beta_n}. \tag{A34}$$

Here, the kernel $K_{\xi\zeta}$ (indices ξ,ζ denote arbitrary combinations of indices α,β) is calculated according to

$$K_{\xi_n\zeta_{n'}} = \int_{t_{n-1}}^{t_n} d\tau \int_{t_{n'-1}}^{t_{n'}} d\tau' \, \Gamma_{\xi_n\zeta_{n'}}(\tau-\tau'), \quad n \neq n', \qquad K_{\xi_n\zeta_n} = \int_{t_{n-1}}^{t_n} d\tau \int_{t_{n-1}}^{\tau} d\tau' \, \Gamma_{\xi_n\zeta_n}(\tau-\tau'), \tag{A35}$$

where

$$\Gamma_{\xi\zeta}(t) = \sum_{\mathbf{q}} \gamma_{\mathbf{q}\xi}\gamma_{\mathbf{q}\zeta}^* \eta_{\mathbf{q}}(t), \tag{A36}$$

and $\gamma_{\mathbf{q}\xi_n}$ are the diagonal elements of the carrier-phonon coupling matrix. Equations (A32)–(A36) define the discretized time evolution of the reduced density matrix in a model with an arbitrary number of carrier states having purely real or imaginary coupling constants. For the two-level model of excitons in a quantum dot the indices α_n, β_n assume only the values 0,1, the phonon coupling is absent in the absence of excitons, i.e., $\gamma_{\mathbf{q},0} = 0$, $\gamma_{\mathbf{q},1} = \gamma_{\mathbf{q}}$, and Eqs. (A32)–(A36) reduce to Eqs. (11)–(15) in the main text.

[1] U. Weiss, *Quantum Dissipative Systems*, 2nd ed. (World Scientific, Singapore, 1999).
[2] A. J. Leggett, S. Chakravarty, A. T. Dorsey, M. P. A. Fisher, A. Garg, and W. Zwerger, Rev. Mod. Phys. **59**, 1 (1987).
[3] N. Makri and D. Makarov, J. Chem. Phys. **102**, 4600 (1995).
[4] N. Makri and D. Makarov, J. Chem. Phys. **102**, 4611 (1995).
[5] E. Sim, J. Chem. Phys. **115**, 4450 (2001).
[6] E. Sim and N. Makri, Chem. Phys. Lett. **249**, 224 (1996).
[7] E. Sim and N. Makri, Comput. Phys. Commun. **99**, 335 (1997).
[8] L. Besombes, K. Kheng, L. Marsal, and H. Mariette, Phys. Rev. B **63**, 155307 (2001).
[9] P. Borri, W. Langbein, S. Schneider, U. Woggon, R. L. Sellin, D. Ouyang, and D. Bimberg, Phys. Rev. Lett. **87**, 157401 (2001).
[10] B. Krummheuer, V. M. Axt, and T. Kuhn, Phys. Rev. B **65**, 195313 (2002).
[11] A. Vagov, V. M. Axt, and T. Kuhn, Phys. Rev. B **66**, 165312 (2002).
[12] P. Machnikowski and L. Jacak, Phys. Rev. B **69**, 193302 (2004).
[13] A. Vagov, V. M. Axt, T. Kuhn, W. Langbein, P. Borri, and U. Woggon, Phys. Rev. B **70**, 201305(R) (2004).
[14] A. J. Ramsay, A. V. Gopal, E. M. Gauger, A. Nazir, B. W. Lovett, A. M. Fox, and M. S. Skolnick, Phys. Rev. Lett. **104**, 017402 (2010).
[15] T. H. Stievater, X. Li, D. G. Steel, D. Gammon, D. S. Katzer, D. Park, C. Piermarocchi, and L. J. Sham, Phys. Rev. Lett. **87**, 133603 (2001).
[16] A. Zrenner, E. Beham, S. Stufler, F. Findeis, M. Bichler, and G. Abstreiter, Nature (London) **418**, 612 (2002).
[17] X. Q. Li, Y. W. Wu, D. Steel, D. Gammon, T. H. Stievater, D. S. Katzer, D. Park, C. Piermarocchi, and L. J. Sham, Science **301**, 809 (2003).
[18] X. D. Xu, B. Sun, P. R. Berman, D. G. Steel, A. S. Bracker, D. Gammon, and L. J. Sham, Science **317**, 929 (2007).
[19] B. Patton, W. Langbein, U. Woggon, L. Maingault, and H. Mariette, Phys. Rev. B **73**, 235354 (2006).
[20] A. Greilich, S. E. Econonou, S. Spatzek, D. R. Yakovlew, D. Reuter, A. D. Wieck, T. L. Reinecke, and M. Bayer, Nature Physics **5**, 262 (2009).
[21] J. Förstner, C. Weber, J. Danckwerts, and A. Knorr, Phys. Rev. Lett. **91**, 127401 (2003).
[22] A. Krügel, V. M. Axt, T. Kuhn, P. Machnikowski, and A. Vagov, Appl. Phys. B **81**, 897 (2005).
[23] A. Krügel, V. M. Axt, and T. Kuhn, Phys. Rev. B **73**, 035302 (2006).
[24] P. Gartner, J. Seebeck, and F. Jahnke, Phys. Rev. B **73**, 115307 (2006).
[25] V. M. Axt, M. Herbst, and T. Kuhn, Superlattices Microstruct. **26**, 117 (1999).
[26] A. Vagov, M. D. Croitoru, V. M. Axt, P. Machnikowski, and T. Kuhn, Phys. Status Solidi B (2011).
[27] B. Krummheuer, V. M. Axt, and T. Kuhn, Phys. Rev. B **72**, 245336 (2005).
[28] E. A. Muljarov and R. Zimmermann, Phys. Rev. Lett. **98**, 187401 (2007).
[29] A. Vagov, M. D. Croitoru, V. M. Axt, T. Kuhn, and F. M. Peeters, Phys. Rev. Lett. **98**, 227403 (2007).
[30] A. Vagov, M. D. Croitoru, V. M. Axt, T. Kuhn, and F. M. Peeters, Phys. Status Solidi B **243**, 2233 (2006).
[31] B. Krummheuer, V. M. Axt, T. Kuhn, I. D'Amico, and F. Rossi, Phys. Rev. B **71**, 235329 (2005).